

Reproducibility and Robustness of a Real-Time Microfluidic Cell Toxicity Assay

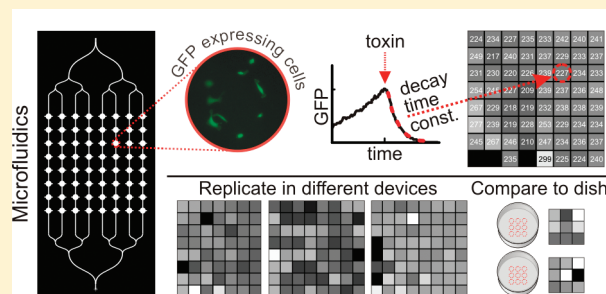
Gregory A. Cooksey,* John T. Elliott, and Anne L. Plant

Biochemical Science Division, NIST, Gaithersburg, Maryland, United States

Supporting Information

ABSTRACT: Numerous opportunities exist to apply microfluidic technology to high-throughput and high-content cell-based assays. However, maximizing the value of microfluidic assays for applications such as drug discovery, screening, or toxicity evaluation will require assurance of within-device repeatability, day-to-day reproducibility, and robustness to variations in conditions that might occur from laboratory to laboratory. This report describes a study of the performance and variability of a cell-based toxicity assay in microfluidic devices made of poly(dimethylsiloxane) (PDMS). The assay involves expression of destabilized green fluorescent protein (GFP) as a reporter of intracellular protein synthesis and degradation.

Reduction in cellular GFP due to inhibition of ribosome activity by cycloheximide (CHX) was quantified with real-time quantitative fluorescence imaging. Assay repeatability was measured within a 64-chamber microfluidic device. Assay performance across a range of cell loading densities within a single device was assessed, as was replication of measurements in microfluidic devices prepared on different days. Assay robustness was tested using different fluorescence illumination sources and reservoir-to-device tubing choices. Both microfluidic and larger scale assay conditions showed comparable GFP decay rates upon CHX exposure, but the microfluidic data provided the higher level of confidence.



Development of robust and quantitative *in vitro* cytotoxicity assays is essential for pharmaceutical safety assessment, reducing animal testing, and evaluating environmental hazards.¹ New technologies such as lab-on-a-chip microfluidic devices are being applied to cytotoxicity studies with the goal of faster, more controlled, and less expensive assays.^{2,3}

The advantages of the use of microfluidics for cell biology applications have been widely discussed.^{4,5} In particular, microfluidic devices typically exhibit small footprints, low reagent consumption, predictable physical properties, real-time control of fluid flow, multiplexing capabilities, low fluorescence background, and the potential for integrated and efficient downstream analyses. These features, which are difficult to achieve in more traditional multiwell culture dishes, can potentially provide significant benefits for high-throughput experimentation such as dose–response screening and cytotoxicity assays, as demonstrated in recent reports.^{6–9}

Reports of microfluidic assays developed to date largely have been focused on miniaturizing and combining benchtop assays and integrating novel microscale functionality. In general, benchmarking the performance of microfluidic cell-based assays has not been emphasized. Establishing reproducibility of microfluidic assays will be essential if they are to be routinely used to generate robust data sets. A challenge with microfluidic assays is that it can be difficult and expensive to produce microdevices that are free from defects, have consistent and stable long-term performance, and are robust to mechanical failure during a cell experiment.^{4,10,11} In addition, microfluidic conditions, such as transport limitations, surface

chemistry effects, and shear forces, may generate environments for cells that are unique from those in larger volume assays and which could reduce reproducibility, robustness, and comparability with larger volume assays.^{12–15} For example, small numbers of living cells may be able to rapidly change the local concentration of nutrients or metabolic products in the small (nanoliter) volumes of microfluidic chambers, requiring continuous perfusion of the cell chambers. In addition, many microfluidic devices for cell culture are prepared from polymers such as poly(dimethylsiloxane) (PDMS). PDMS has many advantageous properties such as ease of use for fabrication, low index of refraction, low contribution to background fluorescence, and flexibility. However, the high surface-to-volume ratios that exist in a microchannel may result in adverse conditions for cells due to the presence of leachables, the porosity and surface chemistry of PDMS may entrap materials, or the gas permeability of PDMS may result in alteration of medium osmolarity or gas content.^{16–18} There are reports that PDMS cell culture chambers do not appear to impact cell or assay behavior,^{6,7,19,20} but some reports have found that cells grown in PDMS microfluidic chambers can behave quite differently than in larger scale culture conditions.^{15,17,18,21–24} Thus, it is possible that the PDMS microfluidic environment may influence the response of cell assays.

Received: February 15, 2011

Accepted: April 4, 2011

Published: April 20, 2011

For this study, we used a previously described toxicity assay that involves expression of green fluorescent protein (GFP) as a reporter of intracellular protein synthesis and degradation.²⁵ A Vero cell line was engineered with the gene for destabilized enhanced GFP under the control of a constitutive cytomegalovirus (CMV) promoter. When ribosomes are inactivated, such as with ricin or cycloheximide (CHX), protein synthesis stops, yet degradation of the GFP by the proteasome continues, leading to a decrease in cellular GFP.

For microfluidics to become routinely utilized in cell experiments, it is necessary that assay performance in devices be reproducible and robust to day-to-day variations and interlaboratory variability. In this report, we studied GFP expression in microfluidic devices with real-time quantitative fluorescence microscopy. We examined within-device variability (repeatability) in parallel microfluidic chambers by monitoring GFP degradation after treatment with a reversible ribosome inhibitor, CHX. The dependence of the assay across a range of cell loading densities within a single device was also explored. We examined device-to-device performance (reproducibility) by replicating measurements in microfluidic devices prepared on different days. Experimental robustness was tested using different fluorescence illumination sources and reservoir-to-device tubing choices, which we found could affect measurements of cell behavior. Finally, the quantitative measurements of GFP degradation rate upon CHX injection in microfluidic devices were compared with results from larger scale culture conditions in 35 mm polystyrene dishes.

MATERIALS AND METHODS

Disclaimer. Certain commercial products are identified in this report to adequately specify the experimental procedure. Such identification does not imply recommendation or endorsement by the National Institute of Standards and Technology, nor does it imply that the materials or equipment identified are necessarily the best available for the purpose.

Device Fabrication and Fluid Connectivity. Microfluidic devices were made out of PDMS (Sylgaard 184, Dow Corning) using soft lithography techniques.²⁶ Details of the fabrication procedure and the fluid delivery system can be found in the Supporting Information. Prior to loading cells, devices were rinsed for at least 1 h with phosphate buffered saline (PBS, Invitrogen Corp.) containing 1% penicillin–streptomycin and Fungizone (PSF, Invitrogen Corp.). To facilitate cell attachment, devices were treated with a 100 $\mu\text{g}/\text{mL}$ fibronectin (FN; F1141, Sigma-Aldrich) solution in PBS for 30 min and subsequently rinsed with medium (CO_2 -independent medium (RR060041, Invitrogen Corp.) with 10% fetal bovine serum (Qualified, Invitrogen Corp.), 2% bovine serum albumin (Sigma-Aldrich), and 1% PSF). Cycloheximide (CHX; Sigma-Aldrich) was diluted to 1 $\mu\text{g}/\text{mL}$ in medium from a 100 mg/mL stock solution in dimethyl sulfoxide.

Live-Cell Microscopy. For time-lapse microscopy, the microfluidic device was placed onto an inverted microscope with a computer-controlled motorized stage (Axio Observer Z1, Carl Zeiss MicroImaging Inc. (Zeiss)). The entire system was enclosed by a heated chamber (37 °C, Zeiss). Phase contrast and fluorescence images were acquired in each culture chamber in an automated mode every 20 min with a 10 \times , 0.3 numerical aperture objective (plan-neofluar, Zeiss). Fluorescence images were acquired with either a mercury arc illumination source (1500 ms exposures; HXP-120, Zeiss) or a light emitting diode (2000 ms exposures; LEDC8, Thorlabs, Inc.), a GFP filter set (set 38 HE eGFP, Zeiss), and CCD camera (CoolSNAP HQ², Photometrics). The area of one imaging

field of view was 898 $\mu\text{m} \times 671 \mu\text{m}$, which corresponds to about 60% of the area within a microfluidic chamber.

Cell Loading. The Vero cell line (CCL-81, American Type Culture Collection) transfected with a cytomegalovirus promoter and a destabilized GFP were previously described.²⁵ Due to a Y-shaped junction at the cell inlet, which had a large dead volume at the junction, a gradient of cell density could be established over the first few minutes of loading. From a starting concentration of 2.75×10^6 cells/mL, we were able to create a distribution of cell densities ranging from a few cells to about 200 cells in each 70 nL chamber across the columns of chambers. The flow of cells was stopped once a few cells were observed flowing down the column on the side opposite of the cell injection port. A more uniform cell density across the columns of chambers was established by pulsing the cell loading solution on and off over a period of 10 to 20 min, such as in Experiments B and C (see Figures S-1 and S-3, Supporting Information). Once a working density of cells was achieved, the cell-loading fluid line was pinched closed to allow the cells time to adhere. In Experiment A, no cells were loaded into the left-most column due to a block in the microchannel after the split from column 2. We estimate that the blocked column in Experiment A resulted in column 2 receiving 18% of the flow, columns 3 and 4 each receiving 15% of the flow, and columns 5–8 each carrying 13% of the flow (see Figure S-11, Supporting Information). Flow of culture medium at a rate of about 1 $\mu\text{L}/\text{min}$ was initiated approximately 1 h after seeding. Cells were loaded into tissue culture polystyrene (TCPS; Falcon 353001, BD) and PMDS-coated dishes at a density of 2.5×10^3 cells in 3 mL of culture medium.

The cells were imaged for approximately 20 h under flow of culture medium. After 20–24 h, the flow of culture medium was stopped and flow of 1 $\mu\text{g}/\text{mL}$ CHX was initiated. Approximately 20 h of CHX exposure was followed by rinsing of culture medium to observe recovery of cells from toxin. CHX was introduced into the dishes by removing 1 mL of fluid in the dishes and replacing it with 1 mL of a 3 $\mu\text{g}/\text{mL}$ CHX solution (final concentration of 1 $\mu\text{g}/\text{mL}$). Fresh culture medium replaced CHX-containing medium in the dishes following multiple media exchanges. The volume of culture medium was maintained at 3 mL in the dishes.

Image Processing and Analysis. Microscopy images were analyzed using ImageJ (NIH) and Matlab (The Mathworks, Inc.) analysis routines. Segmenting the GFP-Vero cells was difficult because cytotoxicity reduced the fluorescence of the cells to near background levels. Thus, we monitored the mean fluorescence intensity from the complete field of view centered in each chamber and subtracted the mean intensity from a cell-free region (background) from the mean image intensity of the entire image to account for variation in the background intensity over time. See Supporting Information for details about background intensity correction. The GFP intensity for each field of view was scaled to range from 0 to 1 during the CHX exposure and fit to an exponential equation of the form $f(t) = Ae^{-t/\tau}$, where τ is the time constant of the GFP decay. Fits were determined from the first 15 h (45 frames) of CHX flow.

The number of cells in each chamber for two replicate experiments (microfluidic Experiments A and B and corresponding dish experiments performed in larger volume dishes; see Supporting Information) was determined by manual counting, which was aided by observing temporal sequences from both phase and fluorescence images. Cell doubling time was estimated by fitting an exponential function to the cell count data and finding $\ln 2^*T$, where T is the time constant of the exponential growth function.

Statistical analyses, including 1-way ANOVA, were conducted using standard Matlab algorithms. Matlab curve fitting functions were

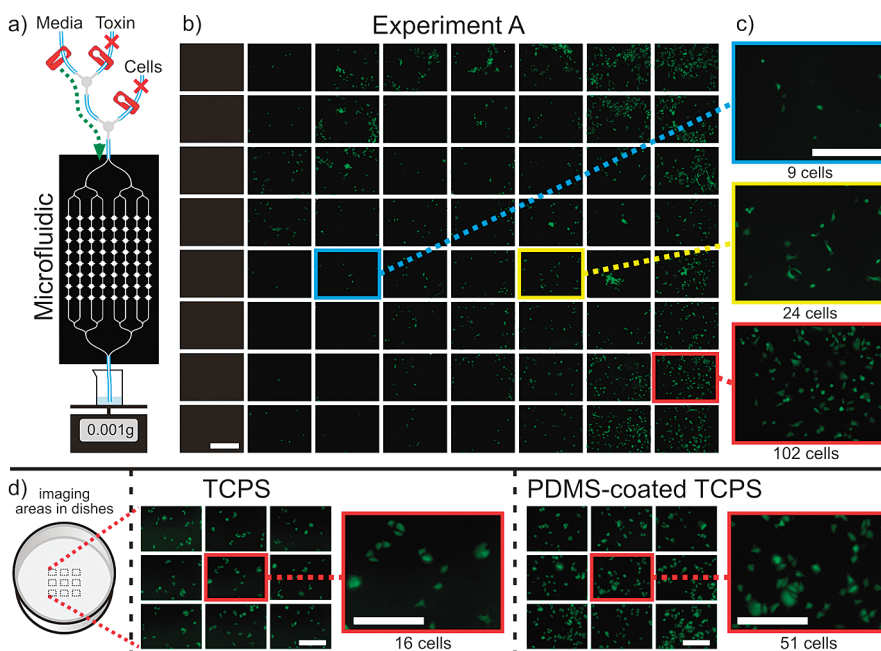


Figure 1. (a) Microfluidic device design and connectivity. Flow paths of normal growth medium and toxin-containing medium merge in a Y-connector (gray), which then joins a fibronectin and cell loading port at a second Y-connector downstream. Pinch clamps (red) are used to open and close fluid flow through any particular fluid line. Fluid enters the device via a single inlet and branches into 8 channels of cell-culture chambers with 8 chambers per column. Each chamber is 1.1 mm in diameter. Fluid leaving the device is collected in a beaker positioned on a microbalance to monitor outflow mass with time. A green arrow shows the open fluid path and red X's denote closed fluid lines during toxin-free media flow. (b) Mosaic image showing fluorescence images of GFP-expressing Vero cells in each chamber at the start of an experiment, approximately 2 h after plating. (c) Enlarged images from 3 chambers with different cell densities: 9 cells (14.9 cells/mm², blue frame), 24 cells (39.8 cells/mm², yellow frame), 102 cells (169 cells/mm², red frame). (d) Illustration of a 35 mm culture dish showing 9 imaging areas (dotted rectangles), mosaic fluorescence image, and enlarged representative fluorescence image for tissue culture polystyrene (TCPS) and PDMS-coated dishes. Scale bars are 400 μ m.

used to calculate exponential decay constants and associated 95% confidence bounds. Curve fitting algorithms were also utilized to estimate the confidence bounds of decay constants as a function of cell density and to estimate cell doubling time.

RESULTS AND DISCUSSION

Device Design. For this study, we designed a simple testbed device with a single inlet and a large number of chambers for cells. The inlet channel branches into 8 columns of chambers, and each column contains eight 1.1 mm diameter chambers for a total of 64 chambers (Figure 1a).

Cell-Based Assay. The cell-based toxicity assay used in these experiments is based on measuring the GFP intensity from a Vero cell line that was transfected with a destabilized GFP driven by a cytomegalovirus promoter. This leads to continuous production of GFP within these cells. Because the GFP construct contains a proteasome targeting sequence, the GFP has a half-life of approximately 2–3 h.^{27,28}

An important potential source of variability in cell assays is the density of cells in a chamber or well. Cell density is of particular concern in microfluidics because chambers can have very small volumes, and the amount of nutrients and metabolites can change dramatically with time and cell number. A gradient of cell densities ranging from 0 to 200 cells/chamber was established in the columns of chambers over the first few minutes of cell loading (see Materials and Methods). Figure 1b shows a mosaic of the GFP fluorescence images of cells from all 64 chambers at 2 h after cell seeding. Enlarged images in Figure 1c

show chambers with relatively low, medium, and high cell densities. Experiment A refers to data acquired from this set of images.

After loading cells into a device, a steady flow of cell culture medium was maintained in the device for approximately 20 h. The total GFP fluorescence in each chamber was measured every 20 min. Figure 2 shows GFP fluorescence intensities of each chamber in the microfluidic device over time. After 20 h, the fluid was switched to continuous flow of 1 μ g/mL CHX. By the end of the first hour of CHX exposure, GFP intensity in each chamber had dropped by approximately 20% on average. The toxin treatment was followed with approximately 20 h of fresh medium rinse to observe cell recovery. Figure 2 shows that GFP intensity could be recovered if cells were washed with fresh CHX-free medium (without toxin), even after approximately 20 h of exposure to a sublethal concentration of CHX. Recovery from CHX is consistent with known reversibility of CHX-inhibited protein synthesis.²⁹ The video in the Supporting Information shows a montage of GFP fluorescence from all culture chambers over the 60 h duration of the experiment.

Assay Repeatability within the Device. The decay in fluorescence intensity within each chamber after addition of CHX was fit to an exponential function, providing a time constant (τ) for GFP degradation during CHX exposure in each chamber. Fits and time constants are shown in each panel of Figure 2. Analysis of the fits yielded an average exponential time constant of 239 ± 17 min (mean \pm standard deviation), with a range from 206 to 281 min. To facilitate visualization, the exponential time constants for each chamber are represented as grayscale blocks within an image according to the chamber's location within the

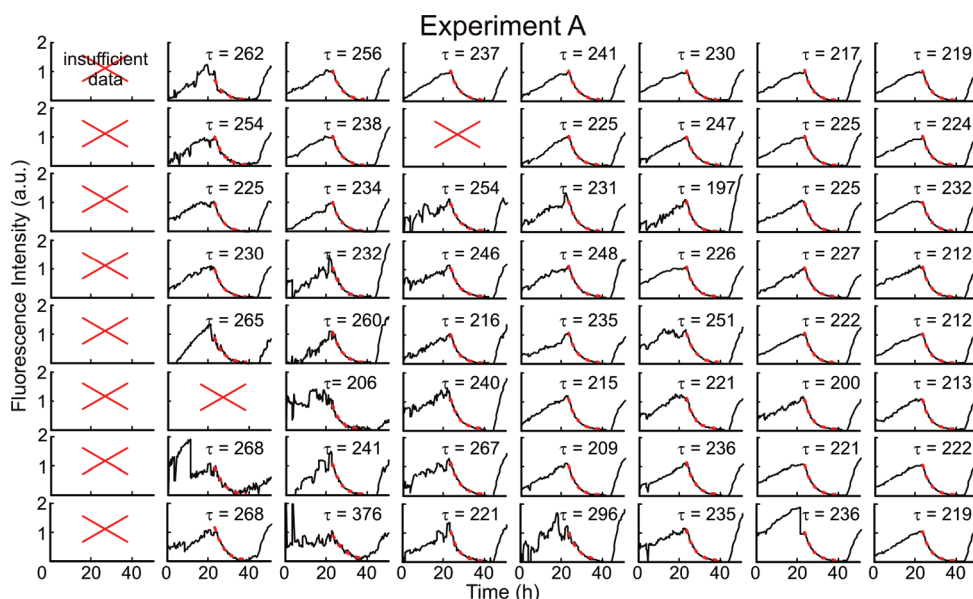


Figure 2. Integrated fluorescence intensity over time (h) from each microfluidic chamber (black traces). Time constants (τ , in min) are listed for the exponential fits (red traces) to the GFP decay during 1 $\mu\text{g}/\text{mL}$ CHX exposure (23 h). Chambers lacking cells or having only a few cells near the edge of the image were not included in the analysis (red X's). Cells were recovered with fresh media at 43 h.

device (Figure 3a). The means and standard deviations of the time constants for each column or row of chambers are shown at the bottom or right of the image, respectively.

Given the small volume and limited growth area within the microfluidic chambers, cell–cell contact,^{30–32} nutrient or toxin depletion, accumulation of secreted factors, or leaching of compounds from PDMS could modify protein expression and/or degradation in a cell-density dependent manner. Furthermore, conditions in upstream chambers could potentially affect cells in downstream chambers due to fluid flow. To study these effects, we examined the time constants to see if they correlated with the cell density or with chamber location within the device. Although the measured time constants varied by at most 18% from the mean, one-way analysis of variance (ANOVA) indicated that the time constants of chambers grouped by column were statistically different ($p < 0.01$). Thus, on average, a potential relationship between cell density and decay time constants cannot be ruled out, as both increased from left to right across the device.

To compare GFP decay time constants to cell density, we manually counted the cell number in each chamber 1 h prior to introduction of toxin. Figure 3b is a display of the cell counts in grayscale blocks according to their corresponding position within the device. Cell densities ranged from 1.7 cells/ mm^2 to nearly 300 cells/ mm^2 . In agreement with the ANOVA result, we find that the mean cell number for each column decreased according to the mean time constant.

Figure 3c shows the time constants for GFP decay plotted against cell density on a chamber-by-chamber basis. The GFP decay time constants in Figure 3c are shown with a smoothed estimate of uncertainty (red dashed line; see Supporting Information). We note that the fitting uncertainty decreased with increasing cell number, which makes comparison of the GFP decay time constant to cell density difficult. In general, the fitting uncertainty drops from about ± 40 min for 1–10 cells in a chamber (1.7 to 17 cells/ mm^2) to ± 10 min for more than 30 cells (50.1 cells/ mm^2) to less than ± 5 min for more than 42 cells

(70.1 cells/ mm^2). Thus, from Figure 3c, it is possible to estimate the precision of the time constant measurement for a given cell density (see Figure S-10, Supporting Information). It appears that a sample of at least 100 cells (167 cells/ mm^2) is necessary to estimate the GFP degradation rate for a population such that the uncertainty due to sampling is less than the uncertainty due to fitting.

While cell density increased by 12-fold across the columns, we measured only a 13% (33 min) decrease in the mean decay time constant as a result. Although we found statistical support for a small dependence of GFP decay with cell density, such a relationship likely has little practical value, at least for this cell and toxin combination, due to the relatively small differences in time constants for low to high cell density and the higher uncertainties for low cell density measurements. Because the cell intensity measurements used in the fitting were derived from the whole image, we believe that the uncertainty in the time constants could be reduced for small numbers of cells by analyzing more limited regions of interest surrounding the cells. Studying variability of single-cell GFP intensity with time is planned for future work. We also aim to get more data regarding dependence on cell density from future studies with different toxins.

Repeatability within the microfluidic device was assessed by analyzing the replicate chambers in each row, which would have the same flow rate and have received a similar concentration of cells during plating. The GFP decay time constant does not appear to depend on the row location of the chamber in the device (ANOVA, $p = 0.27$). This suggests that the response to CHX is not dependent on depletion of nutrients or secretion of signals by cells in upstream chambers.

Assay Robustness and Reproducibility between Devices. To address the issue of reproducibility of the microfluidic assay, we compared results from replicate devices that were fabricated on different days and filled with cells from different passages. We allowed other aspects of the experiment to vary as well, namely, the illumination source and the type of tubing used to connect

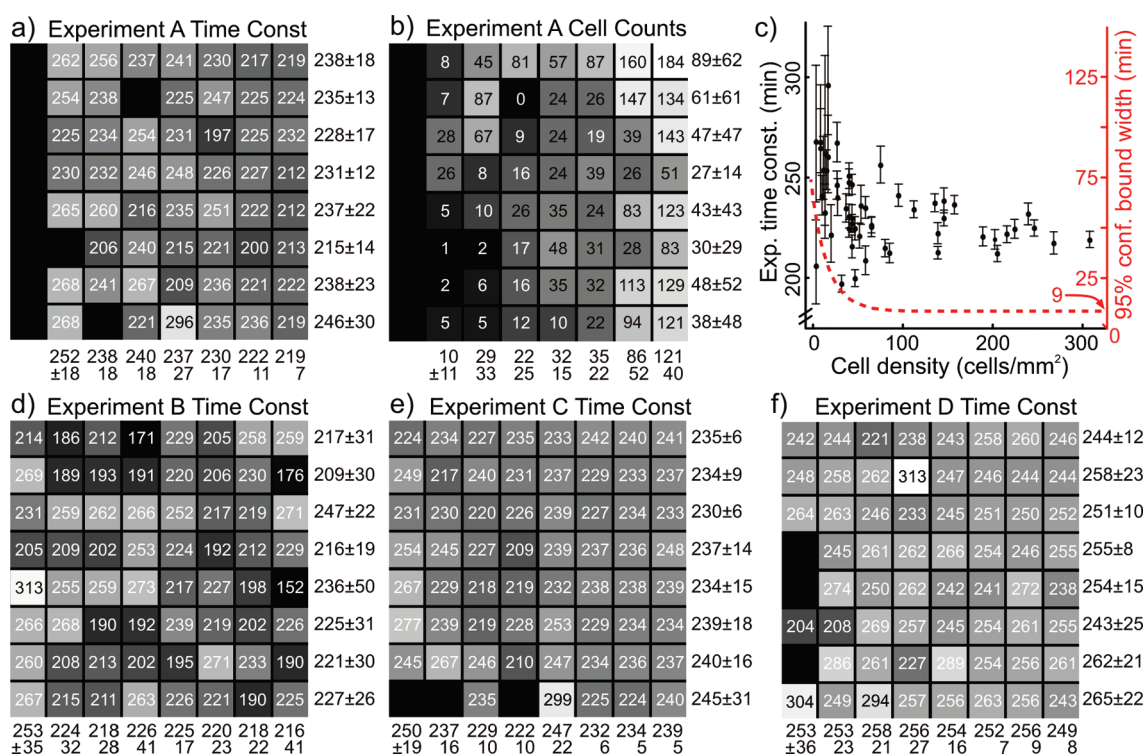


Figure 3. (a) Grayscale image map representing the exponential decay time constants (in min) for the GFP intensity during 1 $\mu\text{g}/\text{mL}$ CHX. The exponential decay time constant (τ , in min) for each chamber is printed in the corresponding location on the image map. Chambers that had insufficient data for fitting are black. The first column of chambers did not receive any cells. Fluid flow direction is downward in each column. (b) Grayscale image map corresponding to the number of cells in each chamber 1 h prior to introduction of 1 $\mu\text{g}/\text{mL}$ CHX. Regions that did not have any cells are black. Contrast was enhanced by raising the grayscale color map to the power $\gamma = 0.4$. (c) Plot of time constant vs cell density (cell count/chamber area) in a field of view) for each chamber. Error bars denote the confidence limits (95%) for the exponential fits to GFP decay during CHX exposure. The right axis (red) shows an estimate of the uncertainty as a function of cell density (dashed red curve), as calculated from a fit to the width of the 95% confidence bounds from each time constant (see Figure S-10, Supporting Information, for more details). (d, e, f) Grayscale image maps of the time constants for replicate experiments. Means \pm standard deviations for the time constants or cell counts from each row and column of culture chambers are shown to the right and below the image maps, respectively. See Table 1 for description of the parameters for each experiment.

fluid reservoirs to the microfluidic device. We have found these variations in experimental setup can lead to differences in measurements. Replicate experiments were acquired with a mercury arc lamp (in contrast to the LED source of Experiment A, above), which had intensity fluctuations that needed to be corrected before fluorescence decay time constants could be accurately estimated. Signal-to-noise ratio measurements from LED and mercury arc lamp excitation are presented in Table S-1, Supporting Information.

Experiments C and D were conducted using Tygon tubing, which is often used due to its transparency and flexibility. However, we have found that medium stored for several hours in Tygon tubing could induce short-lived (lasting approx 1 h) cell shape changes (e.g., blebbing and rounding) upon injection into the microfluidic culture (Experiment D). Because the CHX-containing medium remained stagnant in the tubing for roughly 20 h, we postulate that chemicals leaching from the Tygon tubing or changes in pH or in dissolved gases might have led to the transient shape changes observed in Experiment D. These points remain of great interest for future study. For Experiment C, the medium in the tubing was purged through the cell loading port for several minutes prior to introducing the flow into the microfluidic device, which we believe may be why Experiment C did not show any changes in morphology after switching medium. Teflon tubing was more difficult to work with, but we

did not notice any cell shape changes upon change in medium (Experiments A and B).

Time constants for GFP decay during CHX exposure are shown in Figure 3 d–f for Experiments B, C, and D. Fluorescence images and mean GFP intensity traces over time for each chamber can be found in the Supporting Information. Despite the potential toxic effects of tubing leachables and increased variability in data collected with mercury arc lamp illumination, we found no significant difference in the time course of GFP decay in response to CHX. The measurements of GFP decay under different conditions had small within-experiment variations (the maximum coefficient of variation (CV) was 14%).

A summary of the experimental conditions and the exponential time constants for the cellular response to CHX is presented in Table 1. These data show that the response to CHX as reported by GFP fluorescence decay was highly reproducible and robust to a number of experimental variables. Time constants for the exponential decay of GFP intensity were similar in microfluidic devices fabricated on different days and when different fluorescence illumination sources and/or tubing were used. The mean GFP decay time constant due to exposure to CHX for replicate microfluidic experiments was 237 ± 25 min when all data are pooled. Overall, the CV among the experimental means was 5.3%.

Comparison of Assay in Microfluidic Devices and Larger Scale Conditions. The confined dimensions, limited medium

Table 1. Comparison of Assay Conditions and Summary of Cell Measurements^a

substrate	experiment	tubing	lamp	flow ($\mu\text{L}/\text{min}$)	mean $\tau \pm \text{stdev}$ (min)	n (# regions)	signal-to- noise ratio	cell doubling time (h)
microfluidic	A	Teflon	LED	0.1–1.5	234 \pm 20	52	64 \pm 2	89
	B	Teflon	Hg arc	0.5–3.5	224 \pm 31	63	47 \pm 3	85
	C	Tygon	Hg arc	0.5–2	236 \pm 15	60	48 \pm 3	NM
	D ^b	Tygon	Hg arc	0.5–2	254 \pm 19	61	138 \pm 50	NM
TCPS	A	N/A	LED	N/A bulk	250 \pm 72	8	14 \pm 3	26
	B		Hg arc		239 \pm 48	9	7 \pm 1	25
	C		Hg arc		218 \pm 27	9	9 \pm 0	NM
	D		Hg arc		250 \pm 13	9	9 \pm 2	NM
PDMS	A	N/A	LED	N/A bulk	254 \pm 41	9	11 \pm 1	27
	B		Hg arc		246 \pm 13	9	11 \pm 2	32

^a τ is the time constant for the exponential fit to the decay of GFP intensity due to exposure to 1 $\mu\text{g}/\text{mL}$ CHX. “Experiment” letters designate experiments that were performed on the same day with cells from the same culture passage. See Materials and Methods for descriptions of the measurements and specifics about experimental conditions. Mean τ is the mean exponential time constant from the fits to GFP intensity in all of the chambers or over all fields sampled in larger volume conditions. “Bulk” under the Flow column heading refers to the 3 mL of medium contained in the polystyrene dishes. stdev = standard deviation. NM = not measured. ^b Brief change in cell morphology was observed at start of CHX delivery.

volume, fluid shear, and PDMS substrate of the microfluidic chambers could potentially influence cell behavior, reagent delivery, and perhaps other features of the assay. To compare the performance of the GFP-based assay in a microfluidic device to larger volume conditions, we compared the results of the assay in cells in the microfluidic device with cells in 35 mm TCPS dishes and TCPS dishes coated with approximately 1-mm thick layer of PDMS. The experiments performed under larger volume conditions were completed on the same day and with cells from the same passage as the corresponding microfluidic experiments. Fibronectin coating, cell attachment, and addition and removal of CHX were done at equivalent times to the microfluidic cultures. Fluorescence intensity traces for each field of view with the fitted exponential decay time constants (Figure S-7), the grayscale maps for cell counts (Figure S-8), and comparison of decay time constants as a function of cell density (Figure S-10) can be found in the Supporting Information.

Overall, we find that the microfluidic assays and the assays performed under larger volume conditions produced similar measurements of GFP decay time constants during CHX exposure. However, the confidence bounds for the larger scale conditions were approximately twice as broad as the confidence bounds for the microfluidic measurements of GFP decay (Figure S-10, Supporting Information). This finding indicates that, for a given number of cells, microfluidic devices provide a higher level of confidence in the measurement of CHX-induced GFP decay. These data are summarized in Table 1.

We also compared the sensitivity of the assay to changes in GFP intensity following CHX exposure in microfluidic chambers and larger volume conditions in dishes. Given equivalent number of sampled fields of view (e.g., nine or less), significant changes in GFP were detectable 20–40 min faster in the microfluidic chamber than in the dishes. For example, using any seven fields of view, a significant drop in GFP was determinable in 40, 60, and 80 min for microfluidics, PDMS-coated dishes, and TCPS dishes, respectively. This suggests that the microfluidic assay allows more rapid detection of changes in protein expression following the application of CHX toxin. The lower confidence and slower time to detect significant change in GFP levels in the dish cultures are likely due to the roughly 10-fold higher background autofluorescence of the dish and the large amount of culture medium above the cells. Measurements of the fluorescence

background and signal-to-noise ratio are given in the Supporting Information.

One striking difference between the microfluidic and larger volume assays was the disparity in proliferation rates of the Vero cells. Cell doubling times were significantly shorter in larger volume dishes compared to microfluidic devices, as shown in Table 1 and Figure S-9, Supporting Information. In each of two replicates of cells in microfluidics or in larger scale conditions, cell density was similar for the first 10 h and then began to diverge. The doubling time for cells in dishes was approximately 30 h while the doubling time in the microfluidic device was estimated to be about 90 h. Since larger volume controls included PDMS-coated dishes, we rule out a role for cell–PDMS interactions in the proliferation differences. This does not rule out, however, that materials leaching from the PDMS into the much smaller volumes in the microfluidic chambers could accumulate in higher concentrations and thus significantly impact the cells. Indeed, others have similarly observed much longer proliferation intervals for cells in microfluidics compared to larger volume conditions,^{15,21–23} but these effects are not well characterized and remain important for future studies.

The question of whether microfluidic environments influence assay results requires careful consideration of the culture system and its effects on the assay measurement.^{15,17,19} Thus, cross-platform assay validation is important for interpreting results and relating to more traditional studies in larger scale conditions. For the engineered cell line used in the various conditions reported herein, we have found that the measured decay time constants of GFP degradation by cells exposed to CHX in microfluidic chambers were consistent across replicate experiments. Furthermore, despite a 3-fold difference in proliferation time, GFP degradation rates were indistinguishable from their response in larger volume conditions in dishes.

CONCLUSION

In this study, we examined performance metrics of a live cell-based assay in a microfluidic device. We explicitly evaluated within-device repeatability, between-device reproducibility, and robustness of the microfluidic assay to variations in cell density, illumination sources, and tubing types. Measurements of GFP decay following CHX-induced inhibition of protein synthesis

under these different conditions were found to be consistent. The measurements from microfluidic devices exhibited greater precision than the same measurements performed under traditional larger volume conditions.

Establishment of baseline performance metrics and evaluation of assay robustness are critical for understanding the sources of variability associated with replicating experiments in microfluidic devices. Such metrics should be employed to guide experimental design, implementation of effective controls, and unambiguous interpretation of results from cell-based microfluidic experiments.

■ ASSOCIATED CONTENT

S Supporting Information. Additional information as noted in the text: methods describing microfluidic device fabrication and fluid reservoir connectivity; methods describing background correction and calculation of signal-to-noise ratio; a movie of GFP intensity during growth, CHX-induced protein inhibition, and recovery; figures showing images of cells in microfluidic chambers for each replicate experiment; figures showing measurements of CHX-induced GFP decay time constants in replicate microfluidic devices and dishes; a figure showing temporal recording of flow rate in microfluidic devices; and a figure and table showing measurements and comparison of signal-to-noise ratio for fluorescence measurements in microfluidic devices and dishes. This material is available free of charge via the Internet at <http://pubs.acs.org>.

■ AUTHOR INFORMATION

Corresponding Author

*Tel: 301-975-5529. Fax: 301-975-8246. E-mail: gregory.cooksey@nist.gov

■ ACKNOWLEDGMENT

G.A.C. acknowledges a postdoctoral fellowship from the National Research Council and the American Recovery and Reinvestment Act. We thank Michael Halter, Jim Filliben, and Marc Salit for helpful discussions, Alessandro Tona for maintenance of cell cultures, Glynis Mattheisen for help fabricating devices and counting cells, and Reem Sharaf for counting cells.

■ REFERENCES

- (1) Committee on Toxicity Testing and Assessment of Environmental Agents. *Toxicity testing in the 21st century: A vision and a strategy*; The National Academies Press: Washington, D.C., 2007.
- (2) Wu, M. H.; Huang, S. B.; Lee, G. B. *Lab Chip* **2010**, *10*, 939–956.
- (3) Hong, J.; Edel, J. B.; deMello, A. J. *Drug Discovery Today* **2009**, *14*, 134–146.
- (4) Whitesides, G. M. *Nature* **2006**, *442*, 368–373.
- (5) El-Ali, J.; Sorger, P. K.; Jensen, K. F. *Nature* **2006**, *442*, 403–411.
- (6) Wang, Z.; Kim, M. C.; Marquez, M.; Thorsen, T. *Lab Chip* **2007**, *7*, 740–745.
- (7) Wlodkowic, D.; Faley, S.; Skommer, J.; McGuinness, D.; Cooper, J. M. *Anal. Chem.* **2009**, *81*, 9828–9833.
- (8) Toh, Y. C.; Lim, T. C.; Tai, D.; Xiao, G.; van Noort, D.; Yu, H. *Lab Chip* **2009**, *9*, 2026–2035.
- (9) Wada, K.; Taniguchi, A.; Kobayashi, J.; Yamato, M.; Okano, T. *Biotechnol. Bioeng.* **2008**, *99*, 1513–1517.
- (10) Kim, L.; Toh, Y. C.; Voldman, J.; Yu, H. *Lab Chip* **2007**, *7*, 681–694.
- (11) Whitesides, G. M. *Lab Chip* **2010**, *10*, 2317–2318.

- (12) Paguirigan, A. L.; Beebe, D. J. *Bioessays* **2008**, *30*, 811–821.
- (13) Walker, G. M.; Zeringue, H. C.; Beebe, D. J. *Lab Chip* **2004**, *4*, 91–97.
- (14) Young, E. W. K.; Beebe, D. J. *Chem. Soc. Rev.* **2010**, *39*, 1036–1048.
- (15) Paguirigan, A. L.; Beebe, D. J. *Int. Biol.* **2009**, *1*, 182–189.
- (16) Toepke, M. W.; Beebe, D. J. *Lab Chip* **2006**, *6*, 1484–1486.
- (17) Regehr, K. J.; Domenech, M.; Koepsel, J. T.; Carver, K. C.; Ellison-Zelski, S. J.; Murphy, W. L.; Schuler, L. A.; Alarid, E. A.; Beebe, D. J. *Lab Chip* **2009**, *9*, 2132–2139.
- (18) Lee, J. N.; Jiang, X.; Ryan, D.; Whitesides, G. M. *Langmuir* **2004**, *20*, 11684–11691.
- (19) Bauer, M.; Su, G.; Beebe, D. J.; Friedl, A. *Int. Biol.* **2010**, *2*, 371–378.
- (20) Yin, H.; Patrick, N.; Zhang, X.; Klauke, N.; Cordingley, H. C.; Haswell, S. J.; Cooper, J. M. *Anal. Chem.* **2008**, *80*, 179–185.
- (21) Walker, G. M.; Ozers, M. S.; Beebe, D. J. *Biomed. Microdevices* **2002**, *4*, 161–166.
- (22) Yu, H.; Meyvantsson, I.; Shkel, I. A.; Beebe, D. J. *Lab Chip* **2005**, *5*, 1089–1095.
- (23) Yu, H.; Alexander, C. M.; Beebe, D. J. *Lab Chip* **2007**, *7*, 726–730.
- (24) Millet, L. J.; Stewart, M. E.; Sweedler, J. V.; Nuzzo, R. G.; Gillette, M. U. *Lab Chip* **2007**, *7*, 987–994.
- (25) Halter, M.; Almeida, J. L.; Tona, A.; Cole, K. D.; Plant, A. L.; Elliott, J. T. *Assay Dev. Technol.* **2009**, *7*, 1–9.
- (26) McDonald, J. C.; Duffy, D. C.; Anderson, J. R.; Chiu, D. T.; Wu, H. K.; Schueller, O. J. A.; Whitesides, G. M. *Electrophoresis* **2000**, *21*, 27–40.
- (27) Li, X.; Zhao, X.; Fang, Y.; Jiang, X.; Duong, T.; Fan, C.; Huang, C. C.; Kain, S. R. *J. Biol. Chem.* **1998**, *273*, 34970–34975.
- (28) Halter, M.; Tona, A.; Bhadriraju, K.; Plant, A. L.; Elliott, J. T. *Cytometry A* **2007**, *71*, 827–834.
- (29) Ennis, H. L.; Lubin, M. *Science* **1964**, *146*, 1474–1475.
- (30) Koppers, M.; Ittrich, C.; Faust, D.; Dietrich, C. *J. Cell Biochem.* **2010**, *110*, 1234–1243.
- (31) Eagle, H.; Levine, E. *Nature* **1967**, *213*, 1102–1106.
- (32) Halter, M., unpublished observations of contact-inhibited behavior or GFP-Vero cells.